

# Coronal Mass Ejections - Propagation Time and Associated Internal Energy

P.K. Manoharan<sup>a</sup> and A. Mujiber Rahman<sup>b,1</sup>

<sup>a</sup>*Radio Astronomy Centre, National Centre for Radio Astrophysics,  
Tata Institute of Fundamental Research, Udhagamandalam (Ooty) 643001, India.*

<sup>b</sup>*School of Physics, Madurai Kamaraj University, Madurai 625021, India.*

---

## Abstract

In this paper, we analyze 91 coronal mass ejection (CME) events studied by Manoharan et al. (2004) and Gopalswamy and Xie (2008). These earth-directed CMEs are large (width  $> 160^\circ$ ) and cover a wide range of speeds ( $\sim 120$ – $2400$   $\text{kms}^{-1}$ ) in the LASCO field of view. This set of events also includes interacting CMEs and some of them take longer time to reach 1 AU than the travel time inferred from their speeds at 1 AU. We study the link between the travel time of the CME to 1 AU (combined with its final speed at the Earth) and the effective acceleration in the Sun-Earth distance. Results indicate that (1) for almost all the events (85 out of 91 events), the speed of the CME at 1 AU is always less than or equal to its initial speed measured at the near-Sun region, (2) the distributions of initial speeds, CME-driven shock and CME speeds at 1 AU clearly show the effects of aerodynamical drag between the CME and the solar wind and in consequence, the speed of the CME tends to equalize to that of the background solar wind, (3) for a large fraction of CMEs (for  $\sim 50\%$  of the events), the inferred effective acceleration along the Sun-Earth line dominates the above drag force. The net acceleration suggests an average dissipation of energy  $\sim 10^{31-32}$  ergs, which is likely provided by the Lorentz force associated with the internal magnetic energy carried by the CME.

### *Keywords:*

Coronal Mass Ejections; Propagation of Coronal Mass Ejection;  
Interplanetary Shocks; Interplanetary Coronal Mass Ejections; Travel time

---

<sup>1</sup>on leave from Department of Physics, Hajee Karutha Rowther Howdia College, Uthamapalayam 625533, India.

## 1. Introduction

It is now well established that the major non-recurrent geomagnetic storms are generally associated with the solar wind disturbances generated by fast coronal mass ejections (CMEs). The intensity of such storms primarily depends on the CME size, speed, density, and strength of the southward magnetic field component at the near-Earth space (e.g., Tsurutani et al., 2006). Another aspect of CME-related space weather is large CME-driven interplanetary disturbances that are usually preceded by strong shocks and they are effective accelerators of particles as well as sources of radio emissions. There is a great interest in understanding the propagation characteristics of CMEs and predicting the CME-related space weather. In this connection several studies have been made to investigate (a) the relationship between the speed of the CME at the near-Sun region and effects created by its shock ejecta and/or magnetic cloud at the Earth's magnetosphere (e.g., Richardson et al., 2007), and (b) the arrival times of the CME and its associated shock at 1 AU (e.g., Gopalswamy et al., 2001; 2005; Manoharan et al., 2004). In such recent studies, white-light images mainly obtained from LASCO/SOHO space mission and 1-AU in-situ measurements have been employed.

For example, Gopalswamy et al., (2000) found that in the Sun-Earth distance, CMEs experienced an effective acceleration, which was highly correlated with the initial speed of the CME. They proposed a kinematical model based on the single parameter, i.e., the initial speed of the CME, to predict the arrival time of CME. In subsequent studies (e.g., Gopalswamy et al., 2001, 2005; Manoharan et al., 2004; Michalek et al., 2004), the above model got refined with an acceleration-cessation distance. Since the exact distance at which the effective acceleration ceased was not known, a particular acceleration-cessation distance of 0.76 AU was assumed. However, these empirical models suffer the problem of projected speed of the CME in the coronagraph field of view. Since the initial speed of the CME obtained from the white-light images is in the sky-plane, the speed along the Sun-Earth line is required to predict the travel time of the CME. Therefore, a cone-shaped structure of the CME, instead of the simple geometrical correction, can be assumed to obtain the radial speed of the CME, which then used as an input to the empirical shock arrival (ESA) model to obtain the Sun to Earth travel

time of shocks (Michalek et al., 2004; Xie et al., 2006). The earthward speed employed in these empirical models predicted the travel time within about 75% accuracy (Gopalswamy et al., 2008; Cho et al., 2003, Xie et al., 2006).

Recent studies have however further shown that the radial profile of speed can differ from one CME to the other, depending on the physical properties of the CME (i.e., speed, mass, size, and internal magnetic energy) and the background solar wind in which CME is propagating (e.g., Manoharan 2006, 2010). Additionally, the interaction of a CME with preceding CME(s) can also slow down its propagation and it tends to take longer time to travel to the Earth (i.e., Manoharan et al., 2004). Moreover studies on the evolution of CMEs between Sun and 1 AU, using white-light images and interplanetary scintillation data demonstrated that the internal energy of the CME dominates and contributes to the propagation out to  $\sim 0.35\text{-}0.45$  AU (e.g., Manoharan et al., 2001, 2002; Joshi et al., 2007; Kumar et al., 2010; Manoharan, 2010). The CME evolution model also suggests that the driving Lorentz force caused by the toroidal current overcomes the aero-dynamical drag force applied by the background solar wind within about 0.4 AU (e.g., Chen, 1996). It is likely that the effect of Lorentz force, which depends on the magnetic flux system embedded within the CME, has direct link to the source region of CME on the Sun.

The consequences of the shock associated with a CME at the Earth (e.g., interplanetary shock strength, sudden commencement, and/or sudden impulse) are directly linked to the energy available within the CME. The combined effects of (a) shock strength, (b) magnetic energy within the magnetic cloud, (c) kinetic energy of the ejecta, and (d) physical properties of the background solar wind determine the onset and the intensity of the storm at the Earth's magnetosphere. Therefore the essential part is to understand the relationship between the shock and its driver CME in terms of CME initial and final speeds and travel time over a given distance along the Sun-Earth line. Such an investigation can provide the insight on energy lost/gained by the CME on its way from Sun to 1 AU. For example, a kinematically and/or magnetically weak CME is likely to lose energy on its way and it may not possess sufficient energy to drive a shock ahead of it. In such a situation the shock is likely to detach from the driver CME and dissipate with further time/distance of propagation.

In this paper, we analyze CMEs studied by Manoharan et al., (2004) and Gopalswamy and Xie, (2008) to investigate the link between the travel time of the CME to 1 AU and its initial speed, final speed (also its associated

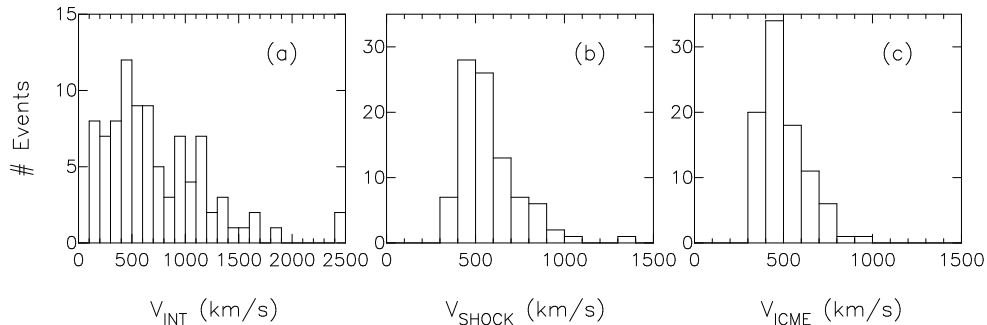


Figure 1: Histograms of (a) initial speed of the CME ( $V_{\text{INT}}$ ) in the LASCO field of view, (b) speed of the associated interplanetary shock at 1 AU ( $V_{\text{SHOCK}}$ ), and (c) speed of the CME at 1 AU ( $V_{\text{ICME}}$ ). It is clearly seen that the wide range of speeds in the LASCO field of view, i.e.,  $\sim 100 - 2400 \text{ km s}^{-1}$ , tends to narrow to a range of  $\sim 400 - 1000 \text{ km s}^{-1}$  at the near-Earth region in the cases of shock and CME.

shock speed) at 1 AU, and its effective acceleration in the Sun-Earth distance. We also consider the distributions of CME initial speed, CME and shock speeds at 1 AU. The paper is organised as follows. Section 2 describes the Earth-directed CME events selected for the study and discusses the correlation between the initial speed of the CME in the sky plane and projection corrected speed. In the next section, the speed of the CME in the near-Earth space has been compared with its travel time in the inner heliosphere. Section 4 provides an account on the average speed of the CME along the Sun-Earth line and discusses the possible internal energy of the CME event. The effective acceleration experienced by the CME events is discussed in Section 5 and the final section gives the summary and conclusion.

## 2. List of Earth-directed CME Events

Manoharan et al., (2004) studied the propagation characteristics of 91 earth-directed CME events, originated close to the central meridian of the Sun (within about  $\pm 30^\circ$  of heliographic latitude and longitude). These CMEs were wide (i.e., halo and partial halo events of width  $> 160^\circ$ ) and accompanied by clear and relatively intense shocks. For each event, the onset of the CME on the Sun was identified by analysing EIT and LASCO images and the arrival of CME-shock pair at 1 AU was examined using the solar wind density, speed, temperature, and interplanetary magnetic field features of the ejecta and magnetic cloud (e.g., low-proton temperature, high-charge state of iron, strong magnetic field, and systematic rotation in field). In the LASCO field

of view, these CMEs covered a speed range of  $V_{\text{INT}} \sim 120\text{--}2400 \text{ km s}^{-1}$ , with an average of  $\sim 730 \text{ km s}^{-1}$ . At 1 AU, Alfvénic Mach numbers of their associated shocks covered a range between 1.1 and 9. The above list included 25 interacting CME events. The criteria to identify the interacting cases were (i) the main fast CME and the preceding slow CME originated from the same active region on the Sun and (ii) the slow CME took off within a day before the main event. The average speed of  $\sim 975 \text{ km s}^{-1}$  of these interacting cases suggests that the subset of fast CMEs could catch up with the slow ones moving ahead.

Figure 1 shows the histograms of (a) initial speeds of CMEs in the LASCO field of view ( $V_{\text{INT}}$ ), (b) in-situ speeds of their corresponding interplanetary shocks ( $V_{\text{SHOCK}}$ ) and (c) interplanetary CMEs at 1 AU ( $V_{\text{ICME}}$ ). At the orbit of the Earth, the speed range of these CME events tends to narrow towards the ambient solar wind (i.e., speed  $\sim 450\text{--}500 \text{ km s}^{-1}$ ). It suggests (1) the effectively slowing down of events resulting because of the interaction between the background solar wind and the CME and (2) the exchange of energy between the CME and ambient solar wind.

### 2.1. Sky-plane and Earthward Speeds

Since the LASCO images provide the sky-plane speed of the CME, Gopalswamy and Xie (2008) computed the speed along the Sun-Earth line. It was found that when the projection was taken into consideration, their empirical shock arrival (ESA) model predicted the arrival of the CME within about 12 hours of uncertainty (also refer to Gopalswamy et al., 2000; 2005). The earthward speeds available for 49 out of 91 events from the list given by Gopalswamy and Xie (2008) have been compared with their simple initial sky-plane speeds obtained from the LASCO images. As shown in Figure 2, the overall correlation between the initial sky-plane speed and the projection-corrected speed is good (i.e., correlation coefficient of  $R \approx 93\%$ ) and the best fit is shown by a continuous line. However, we see a marked difference between two groups of CMEs having speeds in the range, (i)  $V_{\text{INT}} < 900 \text{ km s}^{-1}$  and (ii)  $V_{\text{INT}} > 900 \text{ km s}^{-1}$ . In the high-speed side the scatter is less between the sky-plane speed and projection-corrected speed and the correlation is high,  $\sim 98\%$ . Moreover, the earthward speed shows a systematic downward offset of  $\sim 90 \text{ km s}^{-1}$  (shown by a dotted line at  $V_{\text{INT}} > 900 \text{ km s}^{-1}$ ) with respect to the sky-plane speed. Whereas in the low-speed side ( $< 900 \text{ km s}^{-1}$ ), we see an offset in the positive side,  $\sim 130 \text{ km s}^{-1}$  ( $V_{\text{INT}} < 900 \text{ km s}^{-1}$ ) and on

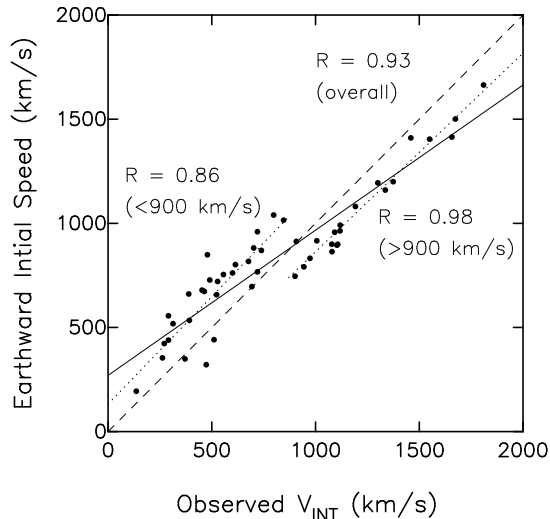


Figure 2: The initial speed of the CME ( $V_{\text{INT}}$ ) in the sky-plane as observed in the LASCO field of view is plotted against its corrected earthward speed as obtained by Gopalswamy and Xie (2008). The dashed line represents the 100% correlation line. The continuous line is the overall best fit to all the data points and provides a correlation coefficient of  $R \sim 93\%$ . The dotted lines are, respectively, best fits to groups of  $V_{\text{INT}} < 900$  and  $V_{\text{INT}} > 900 \text{ km s}^{-1}$  data points and their correlation coefficients are also shown. They show systematic offsets with respect to the 100% correlation line (refer to text).

the average earthward speed is higher than the sky-plane observed speed. In the low-speed side, we see more scatter and the correlation is  $\sim 86\%$ .

Apart from the above discussed 49 disk-centered events, the list given by Gopalswamy and Xie (2008) also included 23 events, which mostly originated at heliographic latitude and longitude  $> |\pm 30^\circ|$ . The comparison of sky-plane and earthward speeds of these non-disk-centered events also shows the downward offset of  $\sim 100\text{--}150 \text{ km s}^{-1}$  with respect to the sky-plane speeds over the entire speed range. The systematic opposite offsets seen, respectively, in the low and high speed regions of the disk-centered events require more investigations. However, for these events the overall agreement between the sky-plane and projection-corrected speeds is good (i.e.,  $R \sim 93\%$ , refer to Figure 2) and in this study, we consider only the initial sky-plane speed obtained from the LASCO images.

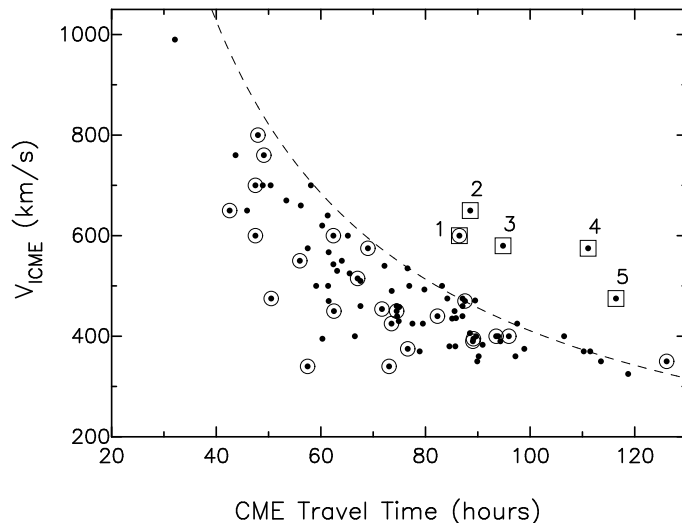


Figure 3: The observed in-situ speed of the CME at the Earth’s orbit is plotted as a function of travel time of the CME between the LASCO field of view and 1 AU. The dashed-line curve shows the estimated travel time assuming that the CME propagated with a constant speed equal to that of its speed at 1 AU ( $V_{ICME}$ ). The points over-plotted with circle symbol are interacting CMEs. Most of the events (except five events shown by square symbols) lie below the assumed-constant speed curve.

### 3. CME Speed at 1 AU

In Figure 3, the speed of the CME at 1 AU ( $V_{ICME}$ ) has been plotted against the travel time of the CME between Sun and Earth. The interacting events have been over-plotted with circle symbols. The continuous dashed line shown in the figure is estimated travel time based on the assumption that the propagation speed of the CME event remained constant at  $V_{ICME}$  in the Sun-Earth distance. It is evident that most of the events fall below the constant-speed curve. It suggests that on the average, these CMEs have travelled faster than the final speed at 1 AU ( $V_{ICME}$ ). Those events lying on the continuous curve or close to it, indicate a nearly-constant speed of propagation in the Sun-Earth line. Another important point to be noted in the above figure is that the value of  $dV/dt$  within  $\sim 70$  hours of travel time is larger than that of events falling in the range  $\sim 70$ -130 hours. The high-speed events ( $V_{ICME} > 500 \text{ km s}^{-1}$ ) show a sharp decline in travel time with the final speed. Whereas events propagating close to the ambient solar wind speed ( $V_{ICME} \leq 500 \text{ km s}^{-1}$ ) show a rather weak dependence of the travel time with speed. It is seen that out of 91 events, 86 events fall close to or below the

constant-speed curve. The comparison of travel time with the constant-speed curve suggests that (1) the initial speed of the CME event should have been higher than its final speed at 1 AU, (2) the aero-dynamical drag force acting on the CME tends to slow down the event, and (3) the exchange of energy between the CME and the ambient solar wind effectively makes the CME to attain the speed of the background solar wind (refer to Figure 1).

In Figure 3, five events show significant positive time offset from the constant-speed curve. These CMEs have particularly taken longer travel times than that corresponding to their speeds at 1 AU (i.e., events falling well above the constant-speed curve are shown by square symbols and marked by numerals 1 to 5 in Figure 3). In these cases, it is likely that they have traveled a considerable portion of the Sun-Earth distance at low speed and a gradual acceleration associated with them have possibly made them to attain a speed faster than the initial speed. The interaction suffered by the event #1 (on June 29, 1999, at 07:31 UT) with the preceding CME has likely modified its speed profile and led to a longer travel time (e.g., Manoharan et al., 2004). In the case of event #2 on July 11, 2000, at 13:27 UT, it has gone through heavy deceleration ( $-43 \text{ ms}^{-2}$ ) in the LASCO field of view. Moreover, the active region associated with this event produced several large and fast CMEs (including the Bastille Day event of 2000) and it is likely that the interaction between CMEs has modified the speed profile in the inner heliosphere. The event #3 corresponds to a CME observed on June 20, 2000 at 09:10 UT. However, as per the recent revision made in the CME catalogue ([http://cdaw.gsfc.nasa.gov/CME\\_list](http://cdaw.gsfc.nasa.gov/CME_list)), it has been found that two events of different speeds ( $455$  and  $635 \text{ kms}^{-1}$ ) have originated in the same location at the same time. Thus, the interaction between these events has affected the propagation. The longer travel times taken by events #4 and #5, respectively, correspond to their low initial speeds of  $266$  and  $192 \text{ kms}^{-1}$  in the LASCO field of view.

#### 4. Travel Time and Average Initial Speed

The travel time of a CME event to the Earth is an indicator of its typical average speed ( $V_{\text{AVG}}$ ) between the LASCO field of view and the Earth. Therefore using a given observed final speed at 1 AU ( $V_{\text{ICME}}$ ), combined with its average speed of propagation in the Sun-Earth distance obtained from the total travel time, it is possible to estimate the expected initial speed of the

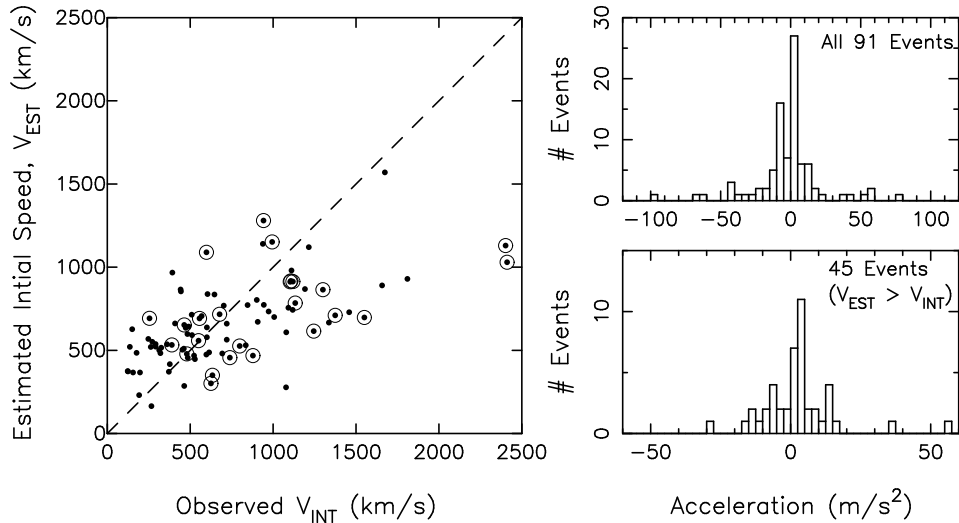


Figure 4: The estimated initial speed ( $V_{EST}$ , refer to equation 1) obtained from the travel time and final speed of the CME at 1 AU ( $V_{ICME}$ ) is compared with the observed initial speed of the CME ( $V_{INT}$ ) in the LASCO field of view. The dashed line indicates the 100% correlation between  $V_{EST}$  and  $V_{INT}$ . The events lying above the line reveal that since  $V_{EST} > V_{INT}$ , these events have been supplied with some excess energy for the propagation and they could overcome the drag force applied by the ambient solar wind. On the other hand, events lying below the line have suffered deceleration and taken more travel time as indicated by  $V_{EST} < V_{ICME}$ . The interacting CME events are marked with circle symbols. On the right-hand side of the plot histograms are shown for (a) effective acceleration of all 91 events in the LASCO field of view and (b) only for 45 events of  $V_{EST} > V_{INT}$ .

CME ( $V_{EST}$ ). The average speed of the CME can be given by,

$$\begin{aligned}
 V_{AVG} &= \left( \frac{\sim 1 \text{ AU}}{\text{CME Travel Time}} \right) \\
 &= \left( \frac{V_{EST} + V_{ICME}}{2} \right).
 \end{aligned} \tag{1}$$

In the above equations, the value of  $V_{EST}$  can be determined from the observed quantities  $V_{ICME}$  and travel time of the CME. Figure 4 displays the correlation plot between the estimated initial speed of the CME ( $V_{EST}$ ) and observed initial ( $V_{INT}$ ) speed in the near-Sun region (i.e., in the LASCO field of view).

#### 4.1. Internal Energy

It is evident from Figure 4 that on the whole the observed initial speeds ( $V_{\text{INT}}$ ) are not well correlated with the estimated speeds ( $V_{\text{EST}}$ ). However, it is interesting to note that nearly 50% of the events (45 events out of 91 events) are located above the correlation line, indicating higher estimated speed than that of the observed initial speed ( $V_{\text{EST}} > V_{\text{INT}}$ ). These events show an average of  $\langle V_{\text{EST}} \rangle \sim 638 \text{ kms}^{-1}$ . However, it is to be noted that the average of these events' observed initial speeds is  $\langle V_{\text{INT}} \rangle \sim 427 \text{ kms}^{-1}$ , which is considerably lower than that of  $\langle V_{\text{EST}} \rangle$ . Since the ambient solar wind speed is considerably lower than  $\langle V_{\text{EST}} \rangle$ , the above result based on the observed travel time (also  $V_{\text{ICME}}$ ) suggests that these events have been supported by an excess energy associated with the CME, i.e., internal magnetic energy, which is revealed in the form of higher estimated initial speed ( $V_{\text{EST}}$ ).

If an average mass for the halo CME events is considered, the average initial estimated speed ( $\langle V_{\text{EST}} \rangle$ ) provides a typical energy of  $\sim 10^{32}$  ergs. It is about 50% larger than the energy associated with the average initial observed speed ( $\langle V_{\text{INT}} \rangle$ ) of the CMEs. Thus, the above exercise suggests that the internal magnetic energy in the range of  $\sim 10^{31-32}$  ergs stored within the CME has been utilized to overcome the drag force and/or transferred to the ambient solar wind. Since the energy to drive a CME phenomenon comes from the 'free energy' available in the magnetic fields of the active region, the currents within the field must support the propagation (e.g., Metcalf et al., 2008). The typical energy dissipated in the Sun-Earth distance is consistent with the two-step deceleration of CME speed profile (i.e., a low or moderate deceleration within  $\sim 0.5$  AU and a rapid deceleration at further large distance) and the support of internal magnetic energy (i.e., Lorentz force) in the propagation of the CME (e.g., Manoharan et al., 2001; Manoharan, 2006; Tokumaru et al., 2000; Howard et al., 2007; Gonzalez-Esparza and Aguilar-Rodriguez, 2009; Chen, 1996).

Whereas the remaining events of lower estimated speed (i.e.,  $V_{\text{EST}} < V_{\text{INT}}$ ; refer to events falling below the correlation line in Figure 4) than the observed initial speed show an opposite trend in averages, respectively,  $\langle V_{\text{EST}} \rangle \sim 682 \text{ kms}^{-1}$  and  $\langle V_{\text{INT}} \rangle \sim 1029 \text{ kms}^{-1}$ . These events in fact have started with a higher initial speed ( $V_{\text{INT}}$ ) than the estimated speed ( $V_{\text{EST}}$ ). But, the observed initial speed and travel time indicate that these events have suffered an effective longer propagation time. In other words, they could not overcome the drag imposed on them by the ambient solar wind and likely decelerated in the Sun-Earth distance. The net effect of simple dragging of

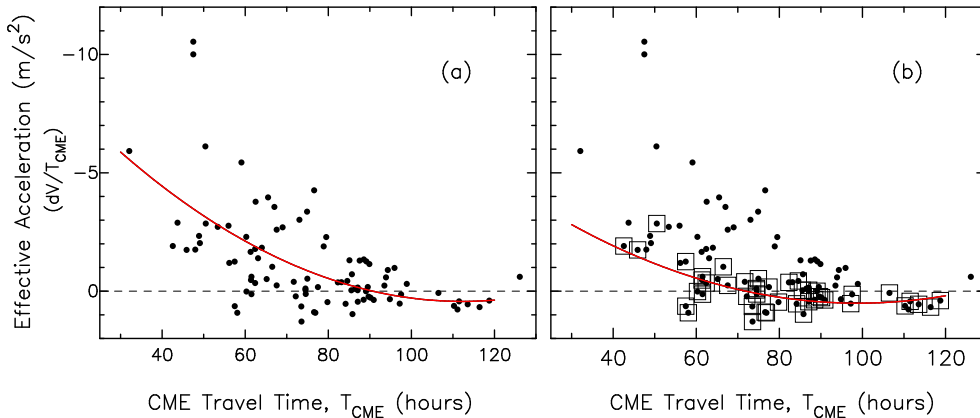


Figure 5: (a) The effective acceleration of the CME as a function of its final speed at 1 AU. The horizontal line defines the constant speed of propagation (i.e., net ‘zero’ acceleration). Events lying below the no effective acceleration line have gone through net positive acceleration and above it have experienced deceleration. (b) same as the above plot and events of  $V_{EST} > V_{INT}$  are shown by over-plotted square symbols.

the CME in the solar wind (i.e., significantly less energy available to overcome the drag force) is indicated by an average lower estimated initial speed than the observed average initial speed ( $\langle V_{EST} \rangle < \langle V_{INT} \rangle$ ).

Additionally, as shown in Figure 4 (right-side panels), the distributions of effective accelerations for all 91 events and events having  $V_{EST} > V_{INT}$  in the LASCO field of view look nearly similar. Whereas, events lying below the correlation line (i.e., remaining 46 events of  $V_{EST} < V_{INT}$ ) show respectively, the average observed initial speed and the average estimated speed of 1029 and 682  $\text{kms}^{-1}$ . It is inferred that these CMEs decelerated heavily due to the interaction between the CME and background solar wind.

Therefore in the group of “ $V_{EST} > V_{INT}$ ” events, the resulting high-estimated speed based on the average speed and observed travel time suggests that these events were supplied with the excess of energy while propagating from Sun to Earth. In other words, their propagation has been supported/aided by the internal energy stored within the CME. Numerical simulations and CME propagation studies have shown that the Lorentz force play a crucial role in supporting the propagation.

## 5. Effective Acceleration

The net effective acceleration of an event measured in the Sun-Earth distance can be given by the change in the speed of the CME divided by its travel time. Figure 5 shows the effective acceleration plotted against the travel time of each event. The dashed horizontal line shows the zero acceleration line, which indicates that the CME traveled at a constant speed. The points lying below this line have gone through an effective positive acceleration and events above it have experienced a net deceleration. When we compare this plot with Figure 3, we see that the high-speed CMEs (or events of small transit time,  $<50$  hours) tend to decelerate heavily than that of the low-speed events. In Figure 5a, the continuous curve is the least-square fit to all the CME events. It provides an average relationship between the effective acceleration experienced by the CME and its travel time in the Sun-Earth distance, as given by,

$$A_{\text{CME}} = -11.3 + 2.1 \times 10^{-1} T_{\text{CME}} - 9.3 \times 10^{-4} T_{\text{CME}}^2, \quad (2)$$

where  $A_{\text{CME}}$  is the effective acceleration (given in  $\text{ms}^{-2}$ ) of the CME and  $T_{\text{CME}}$  (given in hour) is the travel time of the CME in the Sun-Earth distance.

In principle, a CME event traveling with a speed same as the background solar wind (i.e., ambient speed of  $\sim 400 \text{ kms}^{-1}$ ) is expected to show a net zero acceleration and such an event would take  $\sim 103$  hours to travel to 1 AU. But, the least-square fit curve crosses the zero acceleration line at  $\sim 90$  hours and it suggests that on the average CMEs possessed excess energy, which supported in expansion as well as propagation. The above equation also indicates that events taking travel times  $>90$  hours may be accelerated by the solar wind. These results are in agreement with Manoharan, (2006).

In Figure 5b, the set of 45 events, which showed estimated initial speed greater than the observed speed at the LASCO field of view, are shown by over-plotted square symbols. The continuous curve is the best fit to events shown by square symbols (i.e.,  $V_{\text{EST}} > V_{\text{INT}}$ ) and it is given by,

$$A_{\text{CME}} = -6.3 + 1.4 \times 10^{-1} T_{\text{CME}} - 7.0 \times 10^{-4} T_{\text{CME}}^2, \quad (3)$$

where  $A_{\text{CME}}$  and  $T_{\text{CME}}$  are as given in equation (2). The above equation predicts a lesser effective deceleration than the overall curve shown in equation (2). Most of these events (refer to events marked by square symbols in Figure 5b) show positive and/or null acceleration and the decelerating cases on

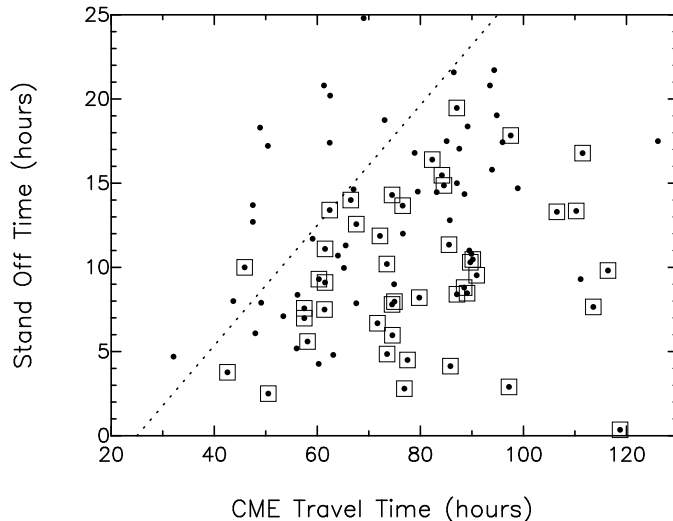


Figure 6: The stand-off time of CME events are compared with their travel time between the LASCO field of view and Earth. The over-plotted square symbol shows event for which the estimated initial speed ( $V_{EST}$ ) is larger than the observed initial speed ( $V_{INT}$ ).

the whole tend to lie close to the zero deceleration line (i.e., within about  $-3 \text{ ms}^{-2}$ ). For these events, the observed travel time and the speed of the CME at 1 AU have revealed the possible associated excess of internal magnetic energy (refer to Section 4) in supporting the propagation. It is likely that the available energy within the CME aids to limit the deceleration in the Sun-Earth distance. It will be interesting to know the source characteristics of these events on the Sun as well as their physical properties at large helio-centric distances (i.e.,  $>1 \text{ AU}$ ). However, points lying above the continuous curve have gone through heavy net deceleration in the Sun-Earth distance. The investigation of absence or considerably less internal energy of these events is also equally important to understand the limited ‘free magnetic energy’ available to drive a CME into the interplanetary medium.

### 5.1. Stand-Off Time

The stand off time of a CME at a distance is given by the time difference between the arrival of CME-driven shock disturbance and the CME at the given distance. Figure 6 shows the stand-off time plotted as a function of travel time of CME to 1 AU. For a given transit time, we see a large scatter between 1 to about 25 hours. In general, a smaller stand-off time indicates that the driver CME and its shock travel closely together. Whereas a large

stand-off time may result as the consequence of CME and shock getting apart due to the less amount of energy available to drive and/or sustain the shock in front of the CME. In the above figure, even at about 40-hours of travel time, the stand-off time ranges between  $\sim 5$  and 20 hours.

In Figure 6, the events having possible excess internal energy (i.e., events of  $V_{\text{EST}} > V_{\text{INT}}$ ) are shown by over-plotted square symbols. The envelop of these events (indicated by a dotted line) at the quickly transiting side shows small stand-off times of  $\leq 10$  hours at the Earth (i.e.,  $T_{\text{CME}} < 50$  hours). Those events travel longer to reach 1 AU (i.e.,  $T_{\text{CME}} > 70$  hours) show stand-off times  $\leq 20$  hours. However, the scatter in the stand-off time with respect to the travel time (and the CME speed at 1 AU,  $V_{\text{ICME}}$ ) is large, which requires more investigations.

## 6. Summary

In this study, we have studied 91 earth-directed CME events analyzed by Manoharan et al., (2004) and Gopalswamy and Xie (2008). These two lists of halo and partial halo CMEs provide a good sample of events, covering a wide range of speeds ( $\sim 100$ – $2500 \text{ km s}^{-1}$ ) in the LASCO field of view. Each event's interplanetary shock and CME have been detected by near-Earth spacecraft. The comparison of the initial speed of the CME with the shock and CME speeds at 1 AU shows that every event experiences the aero-dynamical drag force in the background solar wind and such drag tends to equalize the speed of the CME to that of the solar wind. However, some of the interacting CMEs take longer travel times than that inferred from their final speeds at 1 AU. The interaction tends to slow down the CME.

For about  $\sim 50\%$  of the events (i.e.,  $V_{\text{EST}} > V_{\text{INT}}$ ; 45 out of 91 events), the travel time to 1 AU, combined with the CME's final speed at 1 AU, reveal an effective acceleration in the Sun-Earth distance. This result shows evidence that there is a net supply of energy by the CME to accelerate and support the CME propagation. When the speed associated with a CME is larger than the ambient solar wind, the energy of the CME dominates the influences of the acceleration and/or drag by the background solar wind. The present study suggests an average energy dissipated per event amounts to be about  $\sim 10^{31-32}$  ergs. It is likely that the Lorentz force acting on the CME helps to overcome the drag and to support propagation. However, the amount of energy transferred from the CME to solar wind over a distance range (or a time period) may differ from one event to the other and it is likely

determined by the physical properties of the CME and the local solar wind conditions encountered by the CME on its way. These results are consistent with the two-step deceleration of CME events, i.e., a low or moderate deceleration within  $\sim 0.5$  AU and a rapid deceleration beginning at around  $\sim 0.5$  AU (Manoharan et al. 2001; Manoharan, 2006). Manoharan (2006) demonstrated that the internal energy of the CME contributes to the propagation up to about 0.5 AU.

However, those events experienced net deceleration in the Sun-Earth distance (i.e, for events  $V_{\text{EST}} < V_{\text{INT}}$ ), the driving force is likely absent and/or not significant. Therefore, it is essential to investigate the physical differences between events dominated by the Lorentz force and those ones without it, respectively, on the Sun and in the interplanetary medium.

## Acknowledgements

This work is partially supported by CAWSES-India Phase II program, which is sponsored by the Indian Space Research Organisation (ISRO). A.M.R. acknowledges the facilities and support provided at the Radio Astronomy Centre and he is supported by the FIP Programme (no. F.ETFTNMK040) of the University Grants Commission, New Delhi. We thank G. Agalya for proof reading the manuscript. SOHO (LASCO data) is a project of international collaboration between ESA and NASA.

## References

- [1] Chen, J., 1996. Theory of prominence eruption and propagation: Interplanetary consequences. *Journal of Geophysical Research* 101, 27499-27520.
- [2] Cho, K.-S., Moon, Y.-J., Dryer, M., Fry, C.D., Park, Y.D., Kim., K.-S., 2003. A statistical comparison of interplanetary shock and CME propagation models. *Journal of Geophysical Research* 108(A12),1445. doi:10.1029/2003JA010029.
- [3] Gonzalez-Esparza, A., Aguilar-Rodriguez, E., 2009. Speed evolution of fast CME/shocks with SOHO/LASCO, WIND/WAVES, IPS and in-situ WIND data: Analysis of Kilometric type II emissions. *Annales Geophysics* 27, 3957-3966.

- [4] Gopalswamy, N., Lara, A., Lepping, R.P., Kaiser, M.L., Berdichevsky, D., St. Cyr, O.C., 2000. Interplanetary acceleration of coronal mass ejections. *Geophysical Research Letters* 27, 145.
- [5] Gopalswamy, N., Lara, A., Manoharan, P.K., Howard, R.A., 2005. An empirical model to predict the 1-AU arrival of interplanetary shocks. *Advances in Space Research* 36, 2289.
- [6] Gopalswamy, N., Lara, A., Yashiro, S., Kaiser, M., Howard, R.A., 2001. Predicting the 1-AU arrival times of Coronal Mass Ejections. *Journal of Geophysical Research* 106, 29207–29218.
- [7] Gopalswamy, N., Xie, H., 2008. Comment on Prediction of the 1-AU arrival times of CME-associated interplanetary shocks: Evaluation of an empirical interplanetary shock propagation model by K.-H. Kim et al., *Journal of Geophysical Research* 113, A10105. doi:10.1029/2008JA013030.
- [8] Howard, T.A., Fry, C.D., Johnson, J.C., and Webb, D.F., 2007. On the Evolution of Coronal Mass Ejections in the Interplanetary medium. *Astrophysical Journal* 667, 610-625.
- [9] Joshi, B., Manoharan, P.K., Veronig, A.M., Pant, P., Pandey, K., 2007. Multi-wavelength Signatures of a flare associated Coronal Mass Ejection. *Solar Physics* 242, 143-158.
- [10] Manoharan, P.K., 2006. Evolution of Coronal Mass Ejections in the inner Heliosphere: A study using white-light and scintillation images. *Solar Physics* 235, 345. doi:10.1007/s11207-006-0100-y.
- [11] Manoharan, P.K., 2010. Ooty Interplanetary Scintillation Remote-Sensing Observations and Analysis of Coronal Mass Ejections in the Heliosphere, *Solar Physics* 265, 137-157. doi 10.1007/s11207-010-9593-5.
- [12] Manoharan, P.K., Gopalswamy, N., Yashiro, S., Lara, A., Michalek, G., Howard, R.A., 2004. Influence of Coronal Mass Ejection on propagation of interplanetary shocks. *Journal of Geophysical Research* 109, A06109, doi:10.1029/2003JA010300.

- [13] Manoharan, P.K., Pick, M., 2002, Radio Astronomical Scintillation in the Solar Wind Plasma: Imaging Interplanetary Disturbances. Proceedings of IAU Symposium 199, 426.
- [14] Manoharan, P.K., Tokumaru, M., Pick, M., Subramanian, P., Ipavich, F.M., Schenk, K., Kaiser, M.L., Lepping, R.P., Vourlidas, A., 2001. Astrophysical Journal 559, 1180.
- [15] Metcalf, T.R., De Rosa, M.L., Schrijver, C.J., Barnes, G., Lites, B.W., Georgoulis, M.K., Pevtsov, A.A., Balasubramanian, K.S., Gary, G.A., Jing, J., Li, J., 2008. Non linear Force-Free modeling of coronal magnetic fields. II. Modeling a Filament Arcade and simulated chromospheric and photospheric vector fields. Solar Physics 247, 269-299.
- [16] Michalek, G., Gopalswamy, N., Lara, A., Manoharan, P.K., 2004. Arrival time of halo coronal mass ejections in the vicinity of the Earth. Astronomy and Astrophysics 423, 729, doi:10.1088/0004-637X/710/2/1195.
- [17] Kumar, P., Manoharan, P.K., Wahabuddin., 2010. Evolution of Solar magnetic field and associated multi wavelength Phenomena: Flare events on 2003 November 20. Astrophysical Journal 710, 1195-1204. doi:10.1088/0004-637X/710/2/1195.
- [18] Richardson, I.G., Webb, D.F., Zhang, J., Berdichevsky, D.B., Biesecker, D.A., Kasper, J.C., Kataoka, R., Steinberg, J.T., Thompson, B.J., 2007. Correction to Major geomagnetic storms ( $Dst \leq -100$  nT) generated by corotating interaction regions. Journal of Geophysical Research, Volume 112 ,A12105
- [19] Tokumaru, M., Kojima, M., Fujiki, K., and Yamashita, M., 2000. Three-dimensional propagation of interplanetary disturbances detected with radio scintillation measurements at 327 MHz. Journal of Geophysical Research 105, 10435-10454 .
- [20] Tsurutani, B.T., Gonzalez, W.D., Gonzalez, A.L.C., Guarnieri, F.L., Gopalswamy, N., Grande, M., Kamide, Y., 2006. Corotating solar wind streams and recurrent geomagnetic activity: A review. Journal of Geophysical Research 111, A07S01. doi:10.1029/2005JA011273.

- [21] Xie, H., Gopalswamy, N., Ofman, L., St. Cyr, O.C., Michalek, G., Lara, A., Yashiro, S., 2006. Improved input to the empirical coronal mass ejection (CME) driven shock arrival model from CME cone models. *Space Weather* 4, S10002, doi:10.1029/2006SW000227.